Adaptive Correction for Radiation Patterns of Deformed Phased Array Antenna

BO TANG[1], **JINZHU ZHOU**[1], **BAOFU TANG**[2], **YAN WANG**[1], **AND LE KANG**[1]
[1]Key Laboratory of Electronic Equipment Structure Design, Ministry of Education, Xidian University, Xi'an 710071, China
[2]14th Research Institute of China Electronics Technology Group Corporation, Nanjing 230088, China

Corresponding authors: Jinzhu Zhou (xidian_jzzhou@126.com), Baofu Tang (baofu_tang@126.com), and Le Kang (lkang@xidian.edu.cn)

ABSTRACT The radiation patterns of an active phased array antenna (APAA) will inevitably deteriorate in service, due to the physical deformation of the antenna surface. Therefore, it is crucial that the APAA has an adaptive correction capability for the deterioration of the radiation patterns. This paper investigated an adaptive correction method for the radiation patterns of a deformed APAA, according to a small amount of measured strains from fiber Bragg grating (FBG) sensors. In this method, two kinds of strain-electromagnetic coupling models, which can change the excitation currents of antenna elements, were established using the phase correction and fast Fourier transform, respectively. The strain-electromagnetic coupling models are applied to quickly calculate the adjustment values of excitation currents, and then the corrected excitation currents are sent to the beam control circuit for compensating the influences of the antenna surface deformations. An X-band APAA experimental platform was developed. Some experiments were carried out, and the advantages of two coupling models were also compared and analyzed. The experimental results demonstrated that the proposed method can effectively correct the deterioration of radiation patterns caused by various antenna surface deformations. This method is suitable for developing an adaptive correction system in some applications such as the wing-APAA of an aircraft or the space-based flexible APAA.

INDEX TERMS Active phased array antenna, surface deformation, coupling model, adaptive correction.

I. INTRODUCTION

The shape of an antenna surface, as the boundary condition for electromagnetic wave transmission, directly affects the radiation electromagnetic field of the APAA. However, in practice, the shape of the antenna surface will be changed inevitably due to the external environment loads in service. Antenna surface deformations will seriously affect the radiation performance. For example, it will lead to the reduced antenna gain, beam pointing deviation and side lobe elevation [1]–[3]. Therefore, it is necessary that the APAA has the ability of the adaptive correction for distorted radiation patterns to ensure the reliable operation.

The radiation patterns of a deformed APAA can be adaptively recovered by using the electrical correction method and the mechanical correction method. The mechanical correction method indirectly correct radiation patterns by adaptively

altering the shape of the antenna surface. In the existing study, the shape of the antenna surface can be adjusted using the driving mechanisms [4], or smart materials such as shaped memory alloys [5], [6], magnetic actuators [7], dielectric elastomers [8], and electro-active polymers [9]. However, the mechanisms and actuators require extra installation space, micro-servos, sophisticated control techniques and sustainable power supply, which increases the weight and complexity of the antenna system. In addition, there are also some problems of slow response time and limited correction accuracy in the mechanical correction method.

The electrical correction method for a deformed APAA changes the radiation patterns by adjusting the amplitude and phase of antenna excitation currents. Compared with the mechanical correction method, the electrical correction method can improve the antenna electrical performance without complicated mechanical adjustment mechanism, and it has faster response time, which is more suitable for real-time correction in service. At present, the electrical correction

method for deformed APAA attracts growing interests of many researchers. The projection method [10], fast Fourier transform method [11] and least squares error [12] have been applied to correct the radiation patterns of the deformed APAA. However, the adjustment values of the excitation currents in the aforementioned works are calculated under known deformations. Therefore, they are unable to realize the adaptive correction for radiation patterns in service.

In recent years, the active electrical compensation techniques for deformed APAA have been proposed. The authors in [13] proposes the idea that the electrical performance of a deformed antenna can be corrected by measuring antenna deformation, but they does not give the coupling relationship between the measurement information from sensors and the adjustment values of the antenna excitation currents. There are also some investigations about the adaptive antenna array. For example, a self-adapting flexible antenna array for changing conformal surface is presented in [14], and the radiation patterns are autonomously recovered, according to the measured deformation angles from resistive sensors. However, the adaptive antenna array is not suitable for the compensation of complex deformed shapes in practice, because the deformed shape of antenna surfaces is usually arbitrarily and the accurate antenna surface shape cannot be obtained using the measured angles of resistive sensors. In our previous work, a smart skin antenna was proposed, and the radiation pattern of the deformed skin antenna can be recovered by changing the phase of the excitation current [15]. However, this work does not study the coupling relationship between the amplitude and phase of the excitation currents and measured strains. Moreover, the practical effectiveness of the method needs to be further verified in a practical engineering application.

This paper investigates an adaptive correction method for the radiation patterns of a deformed APAA, according to a small amount of measured strains. Different from our previous work [15], the paper develops a new strain-amplitude and phase coupling model for the adaptive correction. Moreover, a deformable APAA experimental system was developed by using the components and antenna elements from an actual radar system. The aim of the investigation is to evaluate the effectiveness and limits of the strain-phase and the strain-amplitude and phase coupling model for the adaptive correction of distorted radiation patterns. In this paper, two problems are addressed. The first problem is how to build a strain-amplitude and phase coupling model for the adaptive correction method, and the second problem is how to develop a deformable APAA experimental system for realizing the radiation pattern corrections and evaluating the effectiveness and limits of the two coupling models. This investigation is essential as a demonstration of feasibility toward future adaptive correction system in some applications such as the APAA installing into the wings of an aircraft or space-based radar.

Compared with the existing literature [11], [15]–[18], the contributions of this work include:

1) This paper investigated the effectiveness and limits of two coupling models for correcting the distorted radiation patterns. To the best of our knowledge, the effectiveness and limits were studied and validated using a practical experimental system for the first time.

2) A strain-amplitude and phase coupling model, which can calculate adjustment values of the excitation amplitude-phase according to limited strain measurements, were established using the fast Fourier transform algorithm.

3) An X-band deformable APAA experimental system was developed using the components and antenna elements from an actual radar system. Different deformation experiments were carried out, and the corresponding results demonstrated the effectiveness and limits of two coupling models.

The rest of the paper is organized as follows. The problem formulation of the deterioration of radiation patterns caused by the surface deformation is described in Section II. Section III proposes the adaptive correction principle for a deformed APAA, and two strain-electromagnetic coupling models are established. Section IV describes an APAA experimental system with a deformable antenna surface. The experimental results are detailed in Section V. Finally, Section VI concludes the paper.

II. PROBLEM FORMULATION

Suppose a planar APAA with M rows and N columns, and the intervals of array elements are d_x and d_y, respectively. According to the superposition principle of APAA [19], the radiating electric field can be described as follow

$$\boldsymbol{E}(\theta, \phi) = \sum_{m=0}^{M-1} \sum_{n=0}^{N-1} I_{mn} f_{mn}(\theta, \phi) \exp(\mathrm{j}k\boldsymbol{r}_{mn} \cdot \hat{\boldsymbol{r}}) \quad (1)$$

where $I_{mn} = A_{mn} \exp(\mathrm{j}\varphi_{mn})$ is the excitation current of the (m, n) th element, and (m, n) denotes the element of the mth row and the nth column in the planar array. A_{mn} and φ_{mn} denotes the amplitude and phase of the excitation current, respectively. $\boldsymbol{r}_{mn} = [x_{mn}, y_{mn}, z_{mn}]^{\mathrm{T}}$ is the position vector of the (m, n) th element in the array, $f_{mn}(\theta, \phi)$ is the active element pattern, and $\hat{\boldsymbol{r}} = [\sin\theta\cos\phi, \sin\theta\sin\phi, \cos\theta]^{\mathrm{T}}$ is the unitary vector in the radiation direction (θ, ϕ). $k = 2\pi/\lambda$ is the free space propagation constant.

The relative position between elements will be changed due to the antenna surface deformations. Assuming $\Delta\boldsymbol{r}_{mn} = [\Delta x_{mn}, \Delta y_{mn}, \Delta z_{mn}]^{\mathrm{T}}$ is the central position offset of the (m, n) th element, where Δx_{mn}, Δy_{mn} and Δz_{mn} are the central position offset in x, y, z direction, respectively. The radiating electric field after deformation can be expressed as

$$\boldsymbol{E}_s(\theta, \phi) = \sum_{m=0}^{M-1} \sum_{n=0}^{N-1} I_{mn} f_{mn}(\theta, \phi) \exp\left[\mathrm{j}k(\boldsymbol{r}_{mn} + \Delta\boldsymbol{r}_{mn}) \cdot \hat{\boldsymbol{r}}\right]$$

$$(2)$$

Comparing (1) and (2), we can be seen that the phase error will be introduced in the array radiation patterns, when the shape of an antenna surface is changed. Therefore, the electrical performance of APAA will deteriorate. Utilizing the
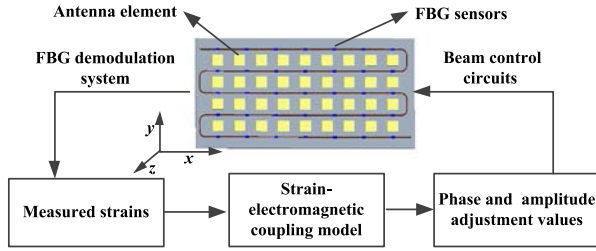
FIGURE 1. Block diagram of adaptive corrections.

principle of the electrical correction, the electrical performance of a deformed APAA can be improved by adjusting the amplitude and phase of the excitation currents. Therefore, the radiating electric field after the correction can be described as follows

$$\tilde{E}_s(\theta, \phi) = \sum_{m=0}^{M-1} \sum_{n=0}^{N-1} I_{mn} \cdot \Delta I_{mn} f_{mn}(\theta, \phi)$$
$$\times \exp\left[jk\left(\boldsymbol{r}_{mn} + \Delta\boldsymbol{r}_{mn}\right) \cdot \hat{\boldsymbol{r}} \right] \quad (3)$$

where $\Delta I_{mn} = \Delta A_{mn} \exp(j\Delta\varphi_{mn})$ is the adjustment value of the excitation current of the (m, n) th element.

From the problem formulation above, it can be concluded that the electrical performance of the deformed APAA can be compensated by inputting appropriate excitation adjustments. Therefore, the key to solve the problem is to establish a relationship between the excitation adjustments and the surface deformations. This paper investigated an adaptive correction method for the radiation patterns of a deformed APAA based on a small amount of strain measurements. The next section provides a detailed description of the correction principle. The surface deformations are characterized using a small amount of strain information measured by FBG sensors, and the adjustments of excitation currents are obtained using the established strain-electromagnetic coupling models.

III. BASIC PRINCIPLE OF ADAPTIVE CORRECTIONS

Fig. 1 depicts the basic principle of the adaptive correction for radiation patterns of a deformed APAA with arranged on a small amount of FBG strain sensors. Firstly, the strains are measured by the FBG strain sensors when the shape of antenna surface is changed. Secondly, inputting the measured strains into the established strain-electromagnetic coupling model, and then the adjustment values of excitation currents will be acquired. Finally, the adjustment values of excitation currents are sent to the beam control circuits to correct the deteriorated radiation patterns. The three steps will be performed automatically in service to achieve the adaptive correction of the distorted radiation patterns.

In the method, the key step is the acquisition of the adjustment values of excitation currents. In this paper, two strain-electromagnetic coupling models were established to calculate the adjustment values of the excitation currents, and the derivation is summarized as follows.

1) Calculate the strains at the FBG sensor locations according to the detected shift of the FBG reflected wavelength;
2) Establish the strain-displacement transformation matrix, and apply the transformation matrix to calculate the central displacements of the antenna elements;
3) Deduce the relationship between the central displacements and the adjustment values of the excitation currents, according to the phase correction and fast Fourier transform, respectively;
4) Combine 2) and 3), the strain-electromagnetic coupling models will be obtained, then the adjustment values of excitation currents can be calculated using the measured strains;
5) Quantify the adjustment values of excitation currents.

A. STRAIN-DISPLACEMENT TRANSFORMATION MATRIX

FBG sensors can be easily pasted on the available space of an antenna panel, because of the characteristic of small size. The reflected wavelength of the FBG sensors arranged on the antenna panel will shift along with the deformation of the antenna surface. Therefore, the strains of the sensor locations can be obtained by detecting the shift of the reflection wavelength. According to the grating theory [20], [21], when the variation of the temperature is little, it is proper to take no account of the effect of the temperature, and then the normal stain ε_l at the location l can be calculated as follow

$$\varepsilon_l = \frac{1}{1 - p_e} \frac{\Delta\lambda_l}{\lambda_l} \quad (4)$$

where p_e is the photo elastic constant of an optical fiber, λ_l and $\Delta\lambda_l$ are the original reflection wavelength and reflection wavelength shift, respectively.

According our previous study [22], the surface deformation can be calculated by a small amount of strains using the established strain-displacement transformation matrix. The central displacements of the elements in z direction for an $M \times N$ APAA can be calculated by the following model

$$\Delta\boldsymbol{z} = \boldsymbol{\Phi}_H \boldsymbol{\Psi}_L^+ \boldsymbol{\varepsilon}_L = \boldsymbol{T}\boldsymbol{\varepsilon}_L \quad (5)$$

where $\Delta\boldsymbol{z} = \left[\Delta z_{00}, \cdots, \Delta z_{mn}, \cdots, \Delta z_{(M-1)(N-1)}\right]^T$ denotes the central position offset of all elements. $\boldsymbol{\Phi}_H \in R^{H \times V}$ is the displacement mode shape matrix at the central position of all elements, $H = M \times N$, and V is the used mode numbers. $\boldsymbol{\varepsilon}_L = [\varepsilon_1, \cdots, \varepsilon_l, \cdots, \varepsilon_L]^T$ is the measured strains at the sensor locations. $\boldsymbol{\Psi}_M^+ \in R^{V \times L}$ represents the pseudo-inverse of the strain mode shape matrix at L sensor locations, and the sensor locations are optimized according to reconstruction accuracy and actual constraints. Therefore, the strain-displacement transformation matrix $\boldsymbol{T}$ can be derived as follows

$$\boldsymbol{T} = \boldsymbol{\Phi}_H \boldsymbol{\Psi}_L^+ \quad (6)$$

B. STRAIN-PHASE COUPLING MODEL

In this subsection, the strain-phase coupling model (SPCM) will be established. It can be seen from (2) that the phase error

$k\Delta\boldsymbol{r}_{mn}\cdot\hat{\boldsymbol{r}}$ is introduced because of the position error of the (m, n) th element for a deformed APAA. The phase error will be eliminated, if the phase adjustment value $\Delta\varphi_{mn}$ of the mn-element satisfies

$$\Delta\varphi_{mn} = -k\Delta\boldsymbol{r}_{mn}\cdot\hat{\boldsymbol{r}} \quad (7)$$

Because the observation direction angle of the unit radial vector $\hat{\boldsymbol{r}}$ is variable during the whole observation space, and the radiation pattern at the beam scanning angle (θ_0, ϕ_0) is usually most concerned, so choosing the unit radial vector of the beam scanning angle (θ_0, ϕ_0) to calculate the phase adjustment. Besides, it can be ignored because the displacement is little in x and y directions, then $\Delta\varphi_{mn}$ can be rewritten as

$$\Delta\varphi_{mn} \approx -k\Delta\boldsymbol{r}_{mn}\cdot\hat{\boldsymbol{r}}_0 \approx -k\cos\theta_0\cdot(\boldsymbol{T}\cdot\boldsymbol{\varepsilon}_L)_{mn} \quad (8)$$

where $\hat{\boldsymbol{r}}_0 = [\sin\theta_0\cos\phi_0, \sin\theta_0\sin\phi_0, \cos\theta_0]^{\mathrm{T}}$ is unit radial vector at beam scanning angle (θ_0, ϕ_0).

C. STRAIN-AMPLITUDE AND PHASE COUPLING MODEL
In this subsection, the strain-amplitude and phase coupling model (SAPCM) is established, which is based on the FFT and inverse FFT algorithm. As described in [11], the excitation current of the deformed APAA is approximately equivalent to add a disturbance of the excitation current to the ideal excitation current. The equivalent excitation current $\tilde{I}_{mn}$ of the deformed APAA with $M \times N$ elements can be expressed as below

$$
\begin{aligned}
&\tilde{I}_{mn}\left(\Delta r_{mn}\right)\\
&= \frac{1}{MN}\sum_{p=0}^{M-1}\sum_{q=0}^{N-1}\left\{\sum_{r=0}^{M-1}\sum_{s=0}^{N-1}I_{rs}\left[1 + jk\left(\Delta x_{rs} - \Delta x_{00}\right)u_p\right.\right.\\
&\quad + jk\left(\Delta y_{rs} - \Delta y_{00}\right)v_q + jk\left(\Delta z_{rs} - \Delta z_{00}\right)\\
&\quad \left.\times\sqrt{1 - u_p^2 - v_q^2}\right]\\
&\quad \left.\times\exp\left[-j2\pi\left(\frac{rp}{M} + \frac{sq}{N}\right)\right]\right\}\exp\left[j2\pi\left(\frac{mp}{M} + \frac{nq}{N}\right)\right] \quad (9)
\end{aligned}
$$

where $u_p = -p\lambda/Md_x$, $v_q = -q\lambda/Nd_y$.

According to the adaptive correction principle proposed by this paper, the structural deformation can be calculated using the measured strains by the established strain-displacement transformation matrix. Considering that the deformation of the antenna surface is mainly z-component. Therefore, the equivalent excitation current can be rewritten as bellow

$$
\begin{aligned}
&\tilde{I}_{mn}\left(\boldsymbol{\varepsilon}_L\right)\\
&\approx \frac{1}{MN}\sum_{p=0}^{M-1}\sum_{q=0}^{N-1}\left\{\sum_{r=0}^{M-1}\sum_{s=0}^{N-1}I_i\left[1 + jk\left((\boldsymbol{T}\cdot\boldsymbol{\varepsilon}_L)_{rs}\right.\right.\right.\\
&\quad \left.- (\boldsymbol{T}\cdot\boldsymbol{\varepsilon}_L)_{00}\right)\times\sqrt{1 - u_p^2 - v_q^2}\Big]\\
&\quad \left.\times\exp\left[-j2\pi\left(\frac{rp}{M} + \frac{sq}{N}\right)\right]\right\}\exp\left[j2\pi\left(\frac{mp}{M} + \frac{nq}{N}\right)\right]\\
&\hspace{10cm}(10)
\end{aligned}
$$

Comparing the equivalent excitation current calculated using (10) with the ideal excitation current, the adjustment

values of the amplitude and phase for the deformed APAA are calculated as bellow

$$
\begin{cases}
\Delta A_{mn} = \mathrm{Abs}\left[\tilde{I}_{mn}\left(\boldsymbol{\varepsilon}_L\right)\right]/\mathrm{Abs}\left(I_{mn}\right)\\
\Delta\varphi_{mn} = \arctan\left[\tilde{I}_{mn}\left(\boldsymbol{\varepsilon}_L\right)\right] - \arctan\left(I_{mn}\right)
\end{cases}
\quad (11)
$$

where $\mathrm{Abs}\left(\cdot\right)$ and $\arctan\left(\cdot\right)$ denote the modulus and argument for plural.

D. QUANTIZATION OF EXCITATION CURRENT ADJUSTMENTS
In practice, the digital phase shifter and attenuator are commonly used to adjust the phase and amplitude of the RF signals. Therefore, the adjustment values of the phase and amplitude need to be quantified. Assuming that the number of bits of the phase shifter and attenuator are t, the actual phase and amplitude adjustment value of the (m, n) th element can be derived as follows

$$
\Delta\varphi'_{mn} = \begin{cases}
b\Delta\varphi_{\min}, & 0 \le \Delta b < 0.5\Delta\varphi_{\min}\\
(b + 1)\Delta\varphi_{\min}, & 0.5\Delta\varphi_{\min} \le \Delta b \le \Delta\varphi_{\min}
\end{cases}
\quad (12)
$$

$$
\Delta A'_{mn} = \begin{cases}
a\Delta A_{\min}, & 0 \le \Delta a < 0.5A_{\min}\\
(a + 1)\Delta A_{\min}, & 0.5A_{\min} \le \Delta a \le A_{\min}
\end{cases}
\quad (13)
$$

where b and a are the round towards nearest integer of the $\Delta\varphi_{mn}/\Delta\varphi_{\min}$ and $-20\log_{10}|\Delta A_{mn}|/\Delta A_{\min}$, Δb and Δa are the remainder of the $\Delta\varphi_{mn}/\Delta\varphi_{\min}$ and $-20\log_{10}|\Delta A_{mn}|/\Delta A_{\min}$, respectively. $\Delta\varphi_{\min} = 2\pi/2^t$ and $\Delta A_{\min} = 1/2^t$ are the minimum quantized shift of the phase and the minimum quantized adjustment of the amplitude, respectively.

IV. EXPERIMENTAL SYSTEM OF DEFORMABLE APAA
To evaluate the effectiveness and limits of two coupling models for the adaptive correction of the distorted radiation patterns, an experimental system of a deformable APAA was developed, and this system consists of a deformable frame, antenna elements, a FBG demodulator system with 70 FBG strain sensors, a power supply, T / R modules and a wave control computer.

Fig. 2 shows the deformable frame of the deformable APAA experimental system, and it mainly consists of a supporting frame, an antenna panel and nine adjusting mechanisms. In the deformable frame, the actuator is used as the adjustment mechanism, and the antenna panel is connected to the supporting frame through nine actuators. The displacement of each actuator is independently controlled, so the complex deformations of the antenna surface can be produced. The maximum displacement of the actuator is 32 mm. The length and width of the antenna panel are 2880 mm and 1728 mm, respectively.

As shown in Fig. 3(a), 70 FBG strain sensors in an optimized configuration were attached 35 locations on the surface of the antenna panel, and each two strain sensors were pasted a location in an orthogonal arrangement. The 35 locations are shown in the Fig. 3(b) [22]. In order to avoid interference
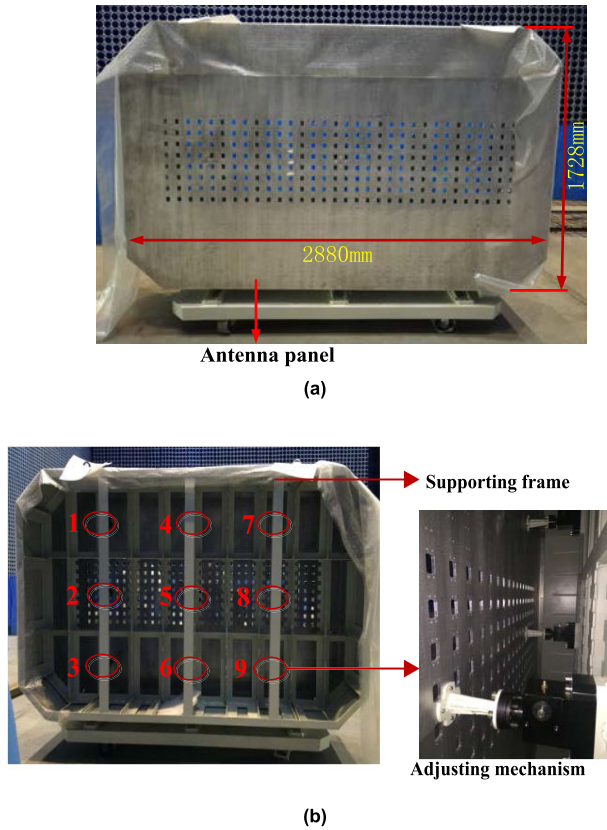
(a)

(b)

FIGURE 2. Deformable frame of the experimental system. (a) Antenna panel without antenna elements. (b) Supporting frame and adjusting mechanism.

(a)

(b)

FIGURE 3. Antenna panel with FBG strain sensors. (a) FBG demodulator system and antenna panel with pasted 70 FBG strain sensors. (b) Sensor placement scheme for 35 sensor locations.

(a)

(b)

FIGURE 4. Experimental measurements. (a) Side view of the experimental system. (b) Back view of the experimental system.

between the FBG strain sensors in the same channel, seven channels of the fiber grating demodulator (si255, Micron Optics, Inc., Atlanta, GA, USA) was employed to acquire the normal strains, and each channel was connected in series with 10 FBG sensors of different Bragg wavelengths.

After the sensors were pasted, 756 horn antennas were assembled on the antenna panel with the spacing of 19.5 mm, as shown in Fig. 4(a). The center frequency of the horn antenna is 10 GHz. In the experiment, due to the limitation of the number of the TR components, the number of the effectively working elements is 256. The antenna panel and horn antenna elements were made of aluminum alloy and they were bolted together. The T / R modules, which can adjust the excitation phase and amplitude of each horn antenna through the digital phase shifter and the digital attenuator, were installed in the supporting frame and connected to the horn antennas through the cable connections. Fig. 4(b) shows the experimental system of the deformable APAA under test in anechoic chamber.

In order to evaluate the correction effectiveness, the radiation patterns are measured under three conditions, which consist of undeformation, deformation and correction. Fig. 4 (a) shows the measurement system, which can obtain the far-field radiation pattern by sampling the radiation field data in the near-field zone according to the theory of the near-far field
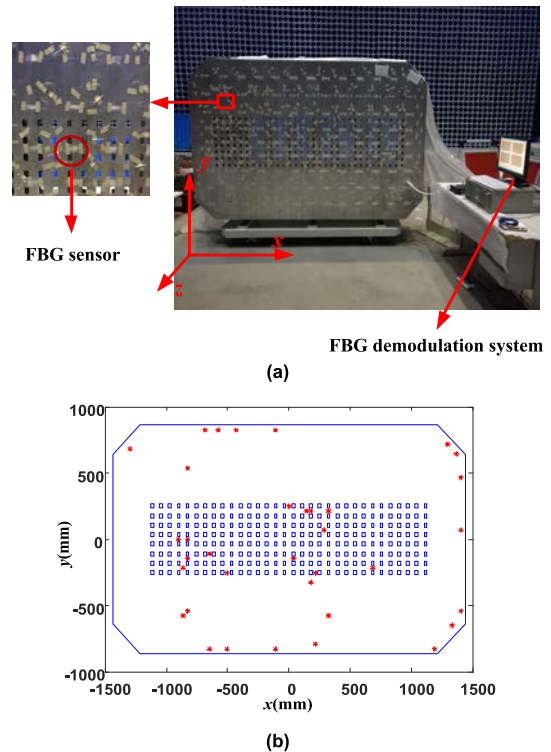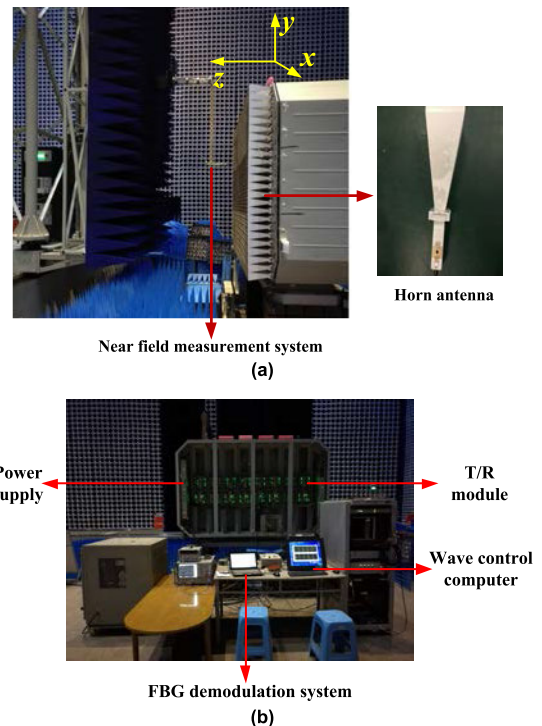
transformation. Because the antenna element used is the high gain horn antenna, its beam width is narrow. When the scanning angle is greater than $\pm 10°$, the maximum
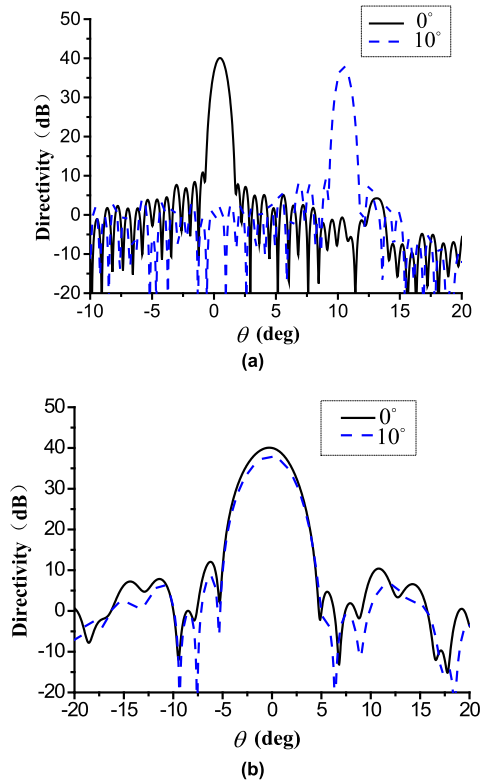
FIGURE 5. Measured patterns under undeformed condition at the scanning angle 0° and 10°. (a) *xoz* plane. (b) *yoz* plane.

FIGURE 6. Calculation results of the saddle bending deformation.

directivity of the APAA will significantly reduce. In addition, there will be large grating lobes in the large scanning angle for the developed experimental system. Therefore, the radiation patterns of the scanning angle at 0° and 10° are selected for the correction experiments. Fig. 5 shows the testing results of the radiation patterns under undeformed condition at scanning angle 0° and 10° in *xoz*-plane ($\phi = 0°$) and *yoz*-plane ($\phi = 90°$), respectively. In order to improve the performance of the antenna system at sidelobe level, the taper distribution of the excitation amplitude is employed. From the testing results, the antenna array has a maximum directivity of 40.09 dB, and the sidelobe level in the *xoz*-plane and *yoz*-plane are about -29.32 and -28.27 dB, respectively, when the beam steers to the scanning angle 0°. At the scanning angle 10°, the maximum directivity is 37.8 dB, and the sidelobe level in the *xoz*-plane and *yoz*-plane are about -29.01 and -29.7 dB, respectively. The detailed electrical performance indexes are presented in Table 1.

TABLE 1. Electrical performance indexes under idea condition.

	$\theta = 0°$		$\theta = 10°$	
	xoz	yoz	xoz	yoz
Directivity (dB)	40.09	40.09	37.8	37.8
Beam direction(°)	0.48	-0.28	10.45	-0.18
Sidelobe level(dB)	-29.32	-28.27	-29.01	-29.7
Beam width (°)	0.94	3.71	0.93	3.83

V. EXPERIMENTAL RESULTS

In this section, the effectiveness and limits of two strain-electromagnetic coupling models are verified using three kinds of deformations, and the correction results were compared and analyzed. The experimental procedures are summarized as follows

1) Changing the shape of the antenna surface by adjusting the displacement of nine actuators, and then measuring the radiation patterns using the near-field measurement.

2) The measured strains at 70 sensors are measured using the FBG demodulation system and then sent to the wave control computer with embedded two strain-electromagnetic coupling models.

3) According to the obtained strains, the wave control computer applies the SPCM and the SAPCM to calculate the adjustment values of the excitation currents, and then send them to the T/R module, respectively. Next, the near-field measurement system measures the corrected radiation patterns, respectively.

A. SADDLE BENDING DEFORMATION

In this subsection, the shape of the antenna surface was changed by adjusting nine actuators to generate the saddle bending deformation. According to the strain information obtained from the FBG demodulator, the shape of the deformed antenna surface, as shown in Fig. 6, can be calculated using (5). Under this deformation condition, the maximum deformation of the antenna element is 10.97 mm, which is 0.36 times of the operating wavelength of the antenna.

Fig. 7 provides the comparisons of the measured radiation patterns at scanning angle 0° in *xoz* plane and *yoz* plane, and the comparisons of the measured radiation patterns at scanning angle 10° in *xoz* plane and *yoz* plane are shown in Fig. 8. The radiation patterns were normalized for the sake of the comparison clearly, and the maximum directivity and other electrical performance indexes are detailed listed in Table 2 and Table 3. Form Fig. 7 and Fig. 8, it is observed that the distorted radiation patterns are almost restored to the undeformed state after the corrections. As shown in Table 2 and Table 3, the maximum directivity corrected by the SPCM and SAPCM increases by 1.32 dB and 1.47 dB at scanning angle 0°, respectively. At scanning
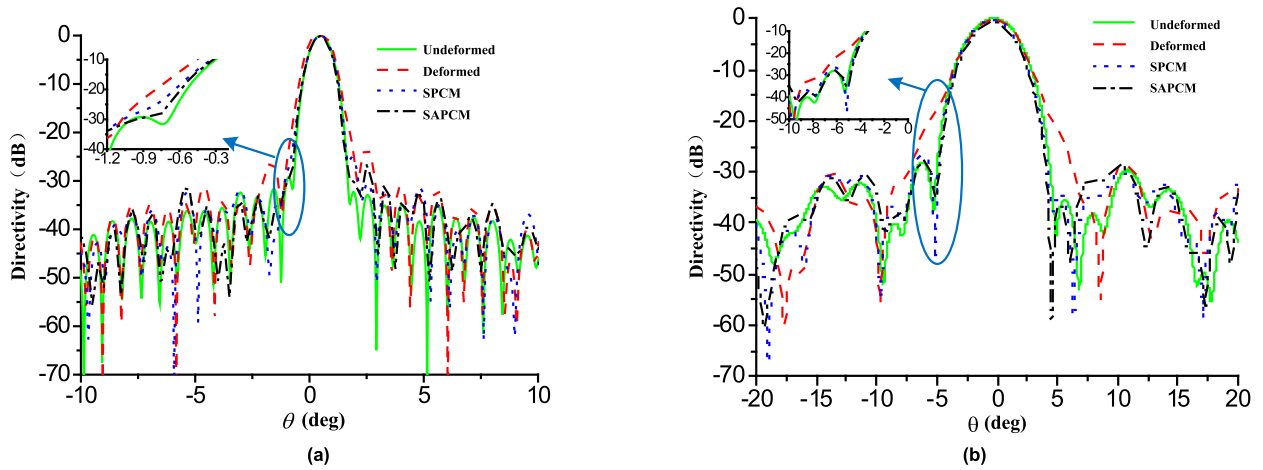
FIGURE 7. Comparison of measured radiation patterns at scanning angle 0°. (a) *xoz* plane. (b) *yoz* plane.
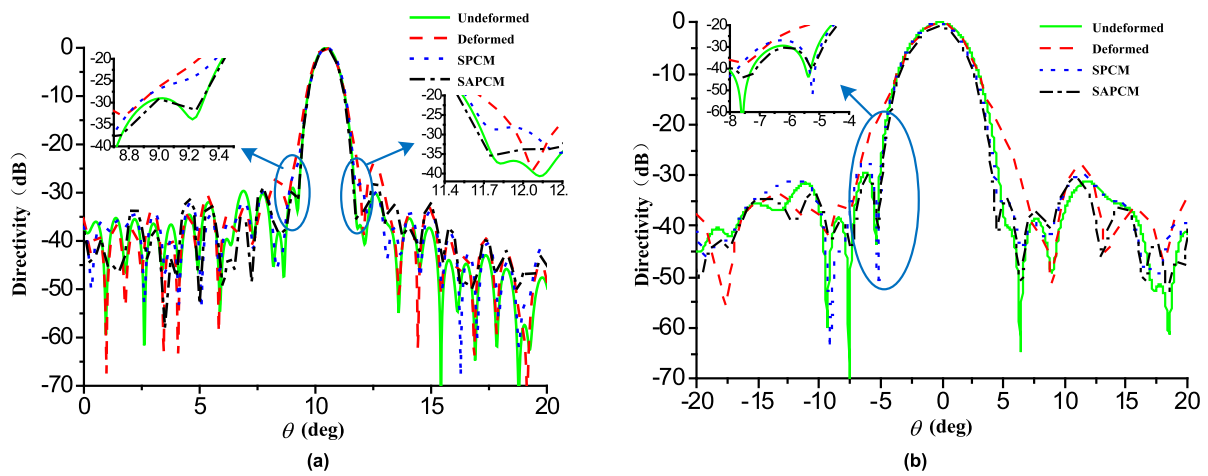

FIGURE 8. Comparison of measured radiation patterns at scanning angle 10°. (a)*xoz* plane. (b) *yoz* plane.

angle 10°, the maximum directivity corrected by the SPCM and SAPCM increases by 1.46 dB and 1.49 dB, respectively. For the sidelobe level, at scanning angle 0°, the sidelobe level corrected with the SAPCM is 1.58 dB and 0.69 dB lower than that corrected with the SPCM in *xoz*-plane and *yoz*-plane, respectively. When the beam steers to the scanning angle 10°, the sidelobe level corrected with the SAPCM is 1.07 dB and 0.56 dB lower than that corrected with the SPCM in *xoz*-plane and *yoz*-plane, respectively. The small zoomed-in plot next to the Fig.7 and Fig. 8 shows that the patterns corrected with the SAPCM are closer to the undeformed patterns than corrected with the SPCM. It can be concluded that the SAPCM has a better correction effect on the sidelobes level of the radiation patterns.

B. BENDING DEFORMATION

The bending deformation is a common deformation of the APAA in service. In this subsection, the antenna panel was changed to generate the bending deformation. Fig. 9 shows
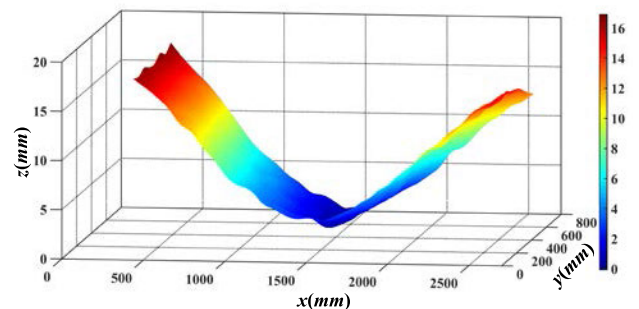

FIGURE 9. Calculation results of the bending deformation.

the shape of the antenna surface calculated using (5). The maximum deformation is 16.87 mm, which is 0.56 times of the operating wavelength of the antenna.

Fig. 10 and Fig. 11 shows the comparisons of the corrected radiation patterns using two strain-electromagnetic coupling models at scanning angle 0° and 10°, respectively.

TABLE 2. Comparison of electrical performance indexes at scanning angle 0°.

	Undeformed		Deformed		SPCM		SAPCM	
	xoz	*yoz*	*xoz*	*yoz*	*xoz*	*yoz*	*xoz*	*yoz*
Directivity (dB)	40.09	40.09	38.6	38.6	39.92	39.92	40.07	40.07
Beam direction (°)	0.48	-0.28	0.45	-0.3	0.5	-0.45	0.5	-0.4
Sidelobe level (dB)	-29.32	-28.27	-24.85	-28.62	-25.09	-25.35	-26.67	-26.04
Beam width (°)	0.94	3.71	1.15	3.63	0.9	3.55	0.95	3.51

TABLE 3. Comparison of electrical performance indexes at scanning angle 10°.

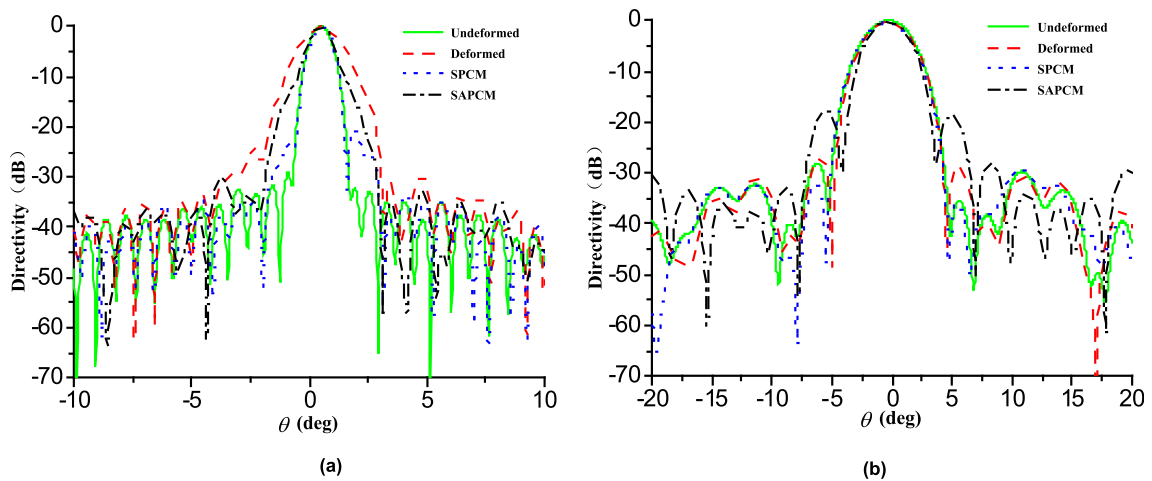|	Undeformed		Deformed		SPCM		SAPCM	
	xoz	*yoz*	*xoz*	*yoz*	*xoz*	*yoz*	*xoz*	*yoz*
Directivity (dB)	37.8	37.8	35.91	35.91	37.37	37.37	37.4	37.4
Beam direction (°)	10.45	-0.18	10.43	-0.2	10.5	-0.36	10.5	-0.25
Sidelobe level (dB)	-29.01	-29.7	-24.03	-28.35	-26.17	-26.47	-27.24	-27.03
Beam width (°)	0.93	3.83	0.96	3.6	0.96	3.6	0.9	3

FIGURE 10. Comparison of measured radiation patterns at scanning angle 0°. (a) *xoz* plane. (b) *yoz* plane.
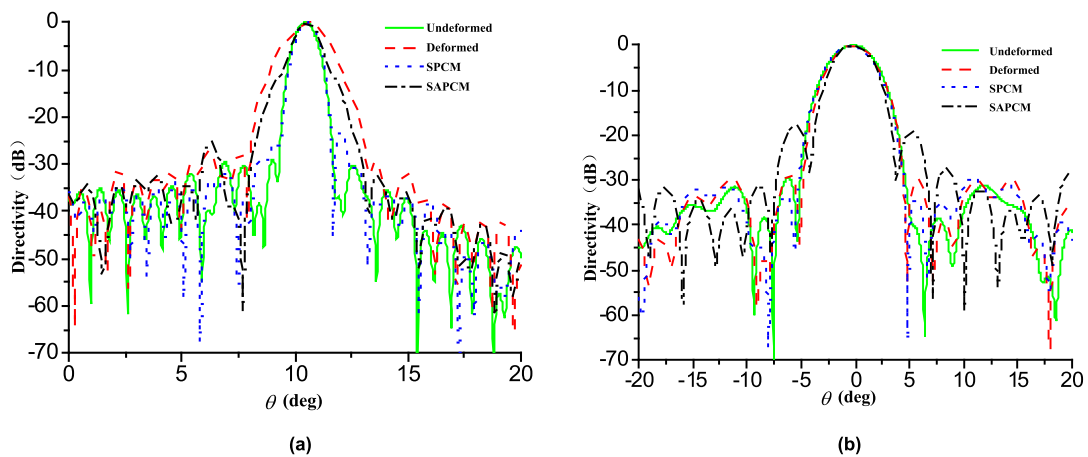

FIGURE 11. Comparison of measured radiation patterns at scanning angle 10°. (a) xoz plane. (b) yoz plane.

The comparisons of the detailed electrical performance indexes are presented in Table 4 and Table 5. Obviously, the SPCM still make the distorted patterns recover to undeformed patterns in the main lobe region, but SAPCM cannot correct the distorted radiation patterns except the maximum directivity. The reason is that the SAPCM uses

TABLE 4. Comparison of electrical performance indexes at scanning angle 0°.

	Undeformed		Deformed		SPCM		SAPCM	
	xoz	*yoz*	*xoz*	*yoz*	*xoz*	*yoz*	*xoz*	*yoz*
Directivity (dB)	40.09	40.09	37.39	37.39	39.37	39.37	39.61	39.61
Beam direction (°)	0.48	-0.28	0.5	-0.28	0.53	-0.48	0.5	-0.3
Sidelobe level (dB)	-29.32	-28.27	-24.81	-28.7	-20.7	-29.08	-30.23	-17.43
Beam width (°)	0.94	3.71	1.55	3.58	0.9	3.5	1	3.23

TABLE 5. Comparison of electrical performance indexes at scanning angle 10°.

	Undeformed		Deformed		SPCM		SAPCM	
	xoz	*yoz*	*xoz*	*yoz*	*xoz*	*yoz*	*xoz*	*yoz*
Directivity (dB)	37.8	37.8	35.45	35.45	37.08	37.08	37.45	37.45
Beam direction (°)	10.45	-0.18	10.55	-0.26	10.53	-0.45	10.5	-0.23
Sidelobe level (dB)	-29.01	-29.7	-27.07	-28.67	-23.13	-23.69	-25.24	-17.83
Beam width (°)	0.93	3.83	1.53	3.65	0.93	3.65	1.03	3.3

the approximation processing in the theoretical derivation. When the Taylor expansion is performed on the phase error, a larger truncation error will occur as the deformation increases.

C. SPOON BENDING DEFORMATION

In this subsection, a larger deformation, whose shape is similar to the spoon bending deformation, was produced by adjusting nine actuators. Fig. 12 shows the reconstruction results of the antenna surface based on limited measured strains. The maximum deformation of the antenna element is 28.3 mm, which is 0.94 times of the operating wavelength.
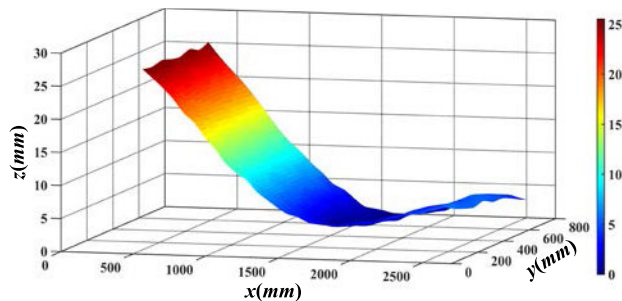

FIGURE 12. Calculation results of spoon bending deformation.

Fig. 13 and Fig. 14 provide the comparisons of the measured radiation patterns. From the corrected results, it can be seen that the SPCM can still effectively correct beam width and maximum directivity in the large deformation. However, the SAPCM is no longer applicable for correcting the distorted patterns in this state of the large deformation, and the corrected patterns with SAPCM are quite different from the unreformed patterns. Table 6 and Table 7 clearly shows the comparisons of electrical performance indexes.

D. DISCUSSION OF EXPERIMENTAL RESULTS

From the experimental results, some discussions are as follows

(1) As for this experiment, with the help of SAPCM, a better correction of the sidelobe level can be obtained compared to that with SPCM, when the maximum deformation of the antenna surface is less than about 0.5 times of the operating wavelength. These results are compared and shown in figs 7~8 and tables 2~3. However, when the maximum deformation exceeds about 0.5 times of the operating wavelength, the SPCM is more effective than the SAPCM, as shown in figs 10~11, 13~14. Therefore, it is suggested that a proper model from the SPCM and SAPCM should be firstly determined to obtain an optimal correction, according to the detected deformation of the APAA in practice. For example, the correction system can automatically select an optimum model from the SPCM and SAPCM, according to a predetermined threshold of the maximum deformation of the APAA measured by FBG sensors.

(2) The experimental results at the scanning angle 0° and 10° are selected in the experiments, because the high-gain horn antennas were applied in the experimental system, the maximum directivity would significantly reduce, when the scanning angle was greater than ±10°. However, the proposed method can be applied to correct the distorted radiation patterns of the APAA with a large scanning range, because the proposed coupling models depend on the scanning range of the array. Moreover, considering the wide applicability of the FBG sensor-based deformation sensing method [22], the proposed method also can be applied to correct the distorted patterns for the APAA with different element types and array size.

(3) Because the coupling model can quickly calculate the adjustment values of the excitation currents, the proposed method is suitable for the real-time correcting of distorted radiation patterns in service. Compared with mechanical correction methods [4, 5] and correction methods based on radiation field sensing [16], the proposed method does not need an adjustment mechanism or an complex measurement system, and the FBG strain sensors can be pasted in available locations on the antenna panel by optimizing the sensor placements. Moreover, unlike the resistive
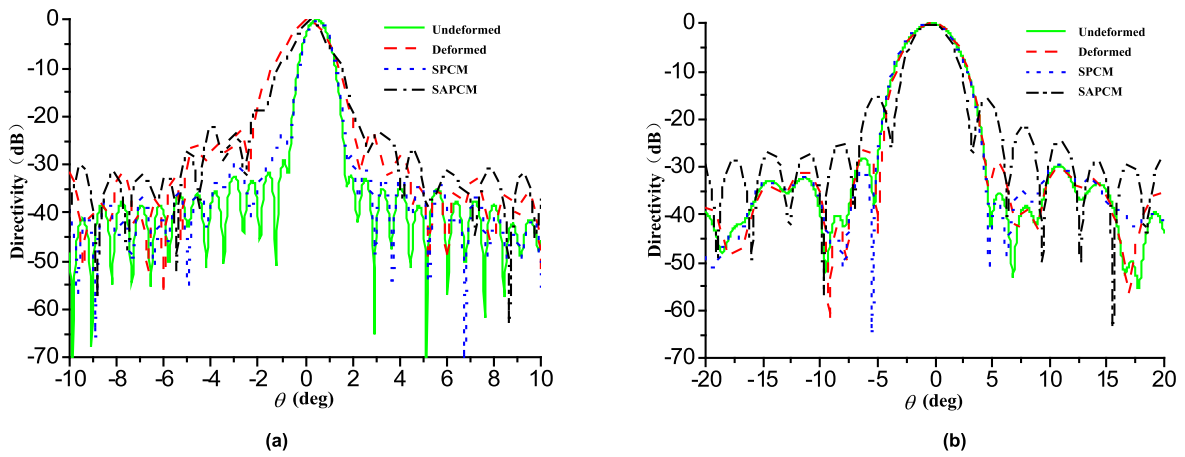
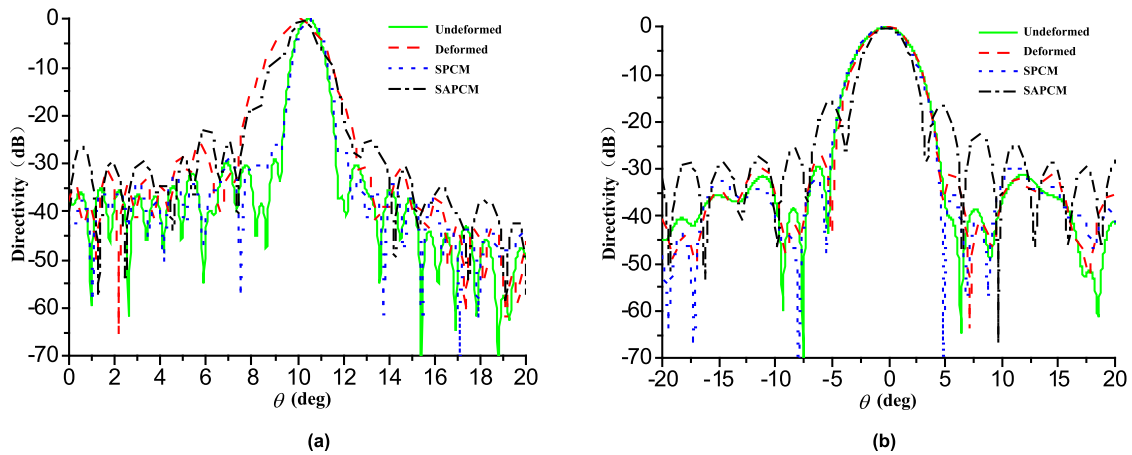**FIGURE 13.** Comparison of measured radiation patterns at scanning angle 0°. (a) *xoz* plane. (b) *yoz* plane.

FIGURE 14. Comparison of measured radiation patterns at scanning angle 10°. (a)*xoz* plane. (b) *yoz* plane.

TABLE 6. Comparison of electrical performance indexes at scanning angle 0°.

	Undeformed		Deformed		SPCM		SAPCM	
	xoz	*yoz*	*xoz*	*yoz*	*xoz*	*yoz*	*xoz*	*yoz*
Directivity (dB)	40.09	40.09	37.88	37.88	39.81	39.81	39.33	39.33
Beam direction(°)	0.48	-0.28	0.1	-0.28	0.53	-0.53	0.2	-0.33
Sidelobe level(dB)	-29.32	-28.27	-22.94	-26.60	-23.87	-29.16	-18.05	-15.17
Beam width (°)	0.94	3.71	1.3	3.7	0.93	3.77	0.99	3.1

TABLE 7. Comparison of electrical performance indexes at scanning angle 10°.

	Undeformed		Deformed		SPCM		SAPCM	
	xoz	*yoz*	*xoz*	*yoz*	*xoz*	*yoz*	*xoz*	*yoz*
Directivity (dB)	37.8	37.8	35.63	35.63	37.65	37.65	37.45	37.45
Beam direction(°)	10.45	-0.18	10.08	-0.2	10.55	-0.43	10.07	-0.2
Sidelobe level(dB)	-29.01	-29.7	-25.85	-27.47	-26.02	-29.64	-18.43	-15.82
Beam width (°)	0.93	3.83	1.38	3.7	0.95	3.75	0.98	3.05

sensor-based method [14], [18], the strain-displacement matrix in equation (6) is suitable for estimating the complex deformation. Therefore, the proposed correction method achieves the adaptive correction of radiation patterns without increasing the complexity of the antenna structure, and it is suitable for developing an adaptive correction system in some applications such as the wing-APAA of an aircraft or the space-based flexible APAA.

VI. CONCLUSION

In this paper, an adaptive correction method, which aims at compensating the deterioration of the radiation patterns caused by the physical deformation of the antenna surface, is studied. The proposed method can adaptively correct the radiation patterns of a deformed APAA. Two strain-electromagnetic coupling models was established to obtain the adjustment values of excitation currents based on a small amount of strains measured by FBG sensors. In addition, an X-band deformable APAA experimental system was designed and fabricated to evaluating the effectiveness and limits of two coupling models. Three kinds of deformation experiments were conducted, and the experimental results demonstrated that the proposed correction method can effectively correct the distorted radiation patterns caused by various physical deformations of the antenna surface. The SAPCM is more suitable for correcting the distorted radiation patterns of the APAA under small deformations. When the antenna deformation is large, the SPCM is preferred. This paper provides a demonstration of feasibility for the APAA with adaptive correction function in the future application, and it also gives some suggestions for selecting the coupling model in an adaptive correction system.

REFERENCES

[1] C. S. Wang, H. Bao, F. S. Zhang, and X. G. Feng, "Analysis of electrical performances of planar active phased array antennas with distorted array plane," *J. Syst. Eng. Electron.*, vol. 20, no. 4, pp. 726–731, Aug. 2009.

[2] E. J. Arnold, J.-B. Yan, R. D. Hale, F. Rodriguez-Morales, and P. Gogineni, "Identifying and compensating for phase center errors in wing–mounted phased arrays for ice sheet sounding," *IEEE Trans. Antennas Propagat.*, vol. 62, no. 6, pp. 3416–3421, Jun. 2014.

[3] C. Wang, M. Kang, W. Wang, B. Duan, L. Lin, and L. Ping, "On the performance of array antennas with mechanical distortion errors considering element numbers," *Int. J. Electron.*, vol. 104, no. 3, pp. 462–484, Mar. 2017.

[4] J. Bernhard, E. Kiely, and G. Washington, "A smart mechanically actuated two-layer electromagnetically coupled microstrip antenna with variable frequency, bandwidth, and antenna gain," *IEEE Trans. Antennas Propag.*, vol. 49, no. 4, pp. 597–601, Apr. 2001.

[5] S. Jalali Mazlouman, A. Mahanfar, C. Menon, and R. G. Vaughan, "Reconfigurable axial–mode helix antennas using shape memory alloys," *IEEE Trans. Antennas Propag.*, vol. 59, no. 4, pp. 1070–1077, Apr. 2011.

[6] S. J. Mazlouman, A. Mahanfar, C. Menon, and R. G. Vaughan, "Square ring antenna with reconfigurable patch using shape memory alloy actuation," *IEEE Trans. Antennas Propag.*, vol. 60, no. 12, pp. 5627–5634, Dec. 2012.

[7] J.-C. Langer, J. Zou, C. Liu, and J. Bernhard, "Micromachined reconfigurable out-of-plane microstrip patch antenna using plastic deformation magnetic actuation," *IEEE Microw. Wireless Compon. Lett.*, vol. 13, no. 3, pp. 120–122, Mar. 2003.

[8] S. Jalali Mazlouman, M. Soleimani, A. Mahanfar, C. Menon, and R. Vaughan, "Pattern reconfigurable square ring patch antenna actuated by hemispherical dielectric elastomer," *Electron. Lett.*, vol. 47, no. 3, pp. 164–165, 2011.

[9] A. Mahanfar, C. Menon, and R. Vaughan, "Smart antennas using electroactive polymers for deformable parasitic elements," *Electron. Lett.*, vol. 44, no. 19, pp. 1113–1114, 2008.

[10] F. Rigobello, G. Mansutti, M. S. Khan, and A.-D. Capobianco, "Pattern recovering of conformal antenna array for strongly deformed surfaces," in *Proc. 11th Eur. Conf. Antennas Propag. (EUCAP)*, Mar. 2017, pp. 869–871.

[11] C. Wang, Y. Wang, J. Zhou, M. Wang, J. Zhong, and B. Duan, "Compensation method for distorted planar array antennas based on structural–electromagnetic coupling and fast Fourier transform," *IET Microw., Antennas Propag.*, vol. 12, no. 6, pp. 954–962, May 2018.

[12] S. Lou, W. Wang, H. Bao, N. Hu, G. Ge, X. Hu, S. Qian, and C. Ge, "A compensation method for deformed array antennas considering mutual coupling effect," *IEEE Antennas Wireless Propag. Lett.*, vol. 17, no. 10, pp. 1900–1904, Oct. 2018.

[13] G. Lesueur, D. Caer, T. Merlet, and P. Granger, "Active compensation techniques for deformable phased array antenna," in *Proc. 3rd Eur. Conf. Antennas Propag.*, Mar. 2009, pp. 1578–1581.

[14] B. D. Braaten, S. Roy, S. Nariyal, M. Al Aziz, N. F. Chamberlain, I. Irfanullah, M. T. Reich, and D. E. Anagnostou, "A self–adapting flexible (SELFLEX) antenna array for changing conformal surface applications," *IEEE Trans. Antennas Propag.*, vol. 61, no. 2, pp. 655–665, Feb. 2013.

[15] J. Zhou, L. Kang, B. Tang, B. Tang, J. Huang, and C. Wang, "Adaptive compensation of flexible skin antenna with embedded fiber Bragg grating," *IEEE Trans. Antennas Propag.*, vol. 67, no. 7, pp. 4385–4396, Jul. 2019.

[16] T. Takahashi, N. Nakamoto, M. Ohtsuka, T. Aoki, Y. Konishi, I. Chiba, and M. Yajima, "On–board calibration methods for mechanical distortions of satellite phased array antennas," *IEEE Trans. Antennas Propag.*, vol. 60, no. 3, pp. 1362–1372, Mar. 2012.

[17] D. Peterman, K. James, and V. Glavac, "Distortion measurement and compensation in a synthetic aperture radar phased-array antenna," Presented at the 14th Int. Symp. Antenna Technol. Appl. Electromagn. Amer. Electromagn. Conf., 2010. [Online]. Available: http://ieeexplore.ieee.org/stamp/stamp.jsp?tp=&arnumber=5552555&isnumber=5552356

[18] P. O'Donovan and A. Rudge, "Adaptive control of a flexible linear array," *Electron. Lett.*, vol. 9, no. 6, p. 121, pp. 121–122, Mar. 1973.

[19] J. Zhou, J. Huang, Q. He, B. Tang, and L. Song, "Development and coupling analysis of active skin antenna," *Smart Mater. Struct.*, vol. 26, no. 2, Feb. 2017, Art. no. 025011.

[20] S. Rapp, L.-H. Kang, J.-H. Han, U. C. Mueller, and H. Baier, "Displacement field estimation for a two-dimensional structure using fiber Bragg grating sensors," *Smart Mater. Struct.*, vol. 18, no. 2, Feb. 2009, Art. no. 025006.

[21] H.-I. Kim, L.-H. Kang, and J.-H. Han, "Shape estimation with distributed fiber Bragg grating sensors for rotating structures," *Smart Mater. Struct.*, vol. 20, no. 3, Mar. 2011, Art. no. 035011.

[22] J. Zhou, Z. Cai, P. Zhao, and B. Tang, "Efficient sensor placement optimization for shape deformation sensing of antenna structures with fiber Bragg strain sensors," *Sensors*, vol. 18, no. 8, p. 2481, Aug. 2018.
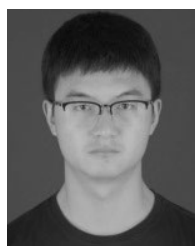
BO TANG received the B.S. degree in mechanical engineering from Xidian University, China, in 2017, where he is currently pursuing the Ph.D. degree. His research interest includes smart skin antenna and active compensation for phased array antenna.

JINZHU ZHOU received the B.S. and M.S. degrees in electromechanical engineering from Northwest A&F University, in 2002 and 2005, respectively, and the Ph.D. degree in mechanical engineering from Xidian University, in 2011.

He is currently a Professor with the Key Laboratory of Electronic Equipment Structure Design, Ministry of Education, Xidian University. He published over 36 articles, and owned 12 patents issued and 13 patents pending. His research interest is in the field of highly integrated phased array antenna. He was a recipient of the 2014 Shaanxi Province Science and Technology Award (First Class) and the Best Paper Award for microwave filters tuning and smart skin antennas at the International Symposium.

BAOFU TANG received the B.S. degree in mechanical engineering from Jiangsu University, and the M.S. degree from the Nanjing University of Science and Technology.

He is currently a Vice Minister with the Antenna Structure Department, Nanjing Research Institute of Electronic Technology, Nanjing, China. He has published more than 20 articles and one book. His research interest is in the field of phased array antenna structure. He received the National Science and Technology Progress Award (First Class).

LE KANG received the B.S. and M.S. degrees from Xidian University, China, in 2008 and 2011, respectively, and the Ph.D. degree in electromagnetic field and microwave technology from the National Key Laboratory of Antennas and Microwave Technology, Xidian University, in 2017. From 2011 to 2012, he was an RF Engineer with Huawei Company, China. He is currently a Lecturer with the School of Mechano-Electronic Engineering, Xidian University. His research interests include wideband antennas, reconfigurable antennas, and phased arrays.

• • •

YAN WANG was born in Shaanxi, China, in 1989. She received the B.S. and M.S. degrees from Xidian University, Xi'an, China, in 2011 and 2014, respectively, where she is currently pursuing the Ph.D. degree with the Key Laboratory of Electronic Equipment Structure Design, Ministry of Education, School of Electromechanical Engineering. Her main research interests include structural-electromagnetic-thermal coupling issue and electromagnetic performance compensation of active phased array antennas.